

# Ex vivo effect of gold nanoparticles on porcine synovial membrane

Raphael Labens,<sup>1,\*</sup> B. Duncan X. Lascelles,<sup>1</sup> Anna N. Charlton,<sup>1</sup> Nicole R. Ferrero,<sup>1</sup> Arnaud J. Van Wettère,<sup>1</sup> Xin-Riu Xia<sup>2</sup> and Anthony T. Blikslager<sup>1</sup>

<sup>1</sup>Center for Comparative Medicine & Translational Research; College of Veterinary Medicine; North Carolina State University; Raleigh, NC USA; <sup>2</sup>Department of Biology; College of Agriculture and Life Sciences; North Carolina State University; Raleigh, NC USA

**Keywords:** gold, nanoparticles, nanogold, synovium, permeability, synovitis, arthritis, ussing, ex vivo

**Abbreviations:** AuNP, gold nanoparticle; AuNPs, gold nanoparticles; LPS, lipopolysaccharide; IL-1 $\beta$ , interleukin-1 $\beta$ ; PGE<sub>2</sub>, prostaglandin E<sub>2</sub>; HA, hyaluronic acid; MMP, matrix metalloproteinase; LDH, lactate dehydrogenase

Gold nanoparticles (AuNPs) have great potential as carriers for local drug delivery and as a primary therapeutic for treatment of inflammation. Here we report on the AuNP-synovium interaction in an ex vivo model of intra-articular application for treatment of joint inflammation. Sheets of porcine femoropatellar synovium were obtained post mortem and each side of the tissue samples was maintained in a separate fluid environment. Permeability to AuNPs of different sizes (5–52 nm) and biomarker levels of inflammation were determined to characterize the ex vivo particle interaction with the synovium. Lipopolysaccharide or recombinant human interleukin-1 $\beta$  were added to fluid environments to assess the ex vivo effect of pro-inflammatory factors on permeability and biomarker levels. The synovium showed size selective permeability with only 5 nm AuNPs effectively permeating the entire tissues' width. This process was further governed by particle stability in the fluid environment. AuNPs reduced matrix metalloproteinase and lactate dehydrogenase activity and hyaluronic acid concentrations but had no effect on prostaglandin E<sub>2</sub> levels. Exposure to pro-inflammatory factors did not significantly affect AuNP permeation or biomarker levels in this model. Results with ex vivo tissue modeling of porcine synovium support an anti-inflammatory effect of AuNPs warranting further investigation.

## Introduction

The medicinal use of gold can be traced back through many centuries, although historical proof for its efficacy is lacking.<sup>1</sup> Today's evidence supports the systemic use of gold salts in man for the treatment of inflammatory arthritis<sup>2–5</sup> but the practical utility is decreased by the potential cytotoxic side effects.<sup>6</sup> There are reports of reduced pain and improved limb use in human and canine patients with arthropathies that receive gold beads implanted at acupuncture sites.<sup>7,8</sup> The suggested beneficial effect is likely attributable to the local liberation of gold ions that can be traced to the surrounding connective tissues.<sup>9</sup>

As an alternative to the use of gold salts or locally applied gold particles, intra-articular administration of gold nanoparticles (AuNPs) has recently been investigated.<sup>10,11</sup> These studies showed that AuNPs reduced synovial pro-inflammatory cytokines and cellular infiltrates and resulted in fewer clinical and radiographic abnormalities in a rodent model of collagen induced arthritis. In addition to a potential primary therapeutic use, AuNPs may also serve as carriers for local drug delivery and thereby increase the half-life of therapeutic levels of select drugs.<sup>12–14</sup> Future

intra-articular application of AuNPs will require specific knowledge of the synovial barrier-carrier interaction, including the permeability of the synovium to nanoparticles. Ex vivo tissue modeling techniques are well established in a variety of biomedical fields and form an important step in advancing bench top discoveries to in vivo applications and ultimately clinical practice.<sup>15,16</sup> Advantages associated with their use include the control and standardization of the experimental environment while maintaining physiologic tissue responses.<sup>17,18</sup> We are not aware of the use of similar techniques as described herein for modeling of synovial pathophysiology. On the basis of these techniques we report on the AuNP-synovium interaction and synovial membrane permeation for potential future intra-articular application in treating arthritis. We hypothesized that by using ex vivo tissue modeling methods we could evaluate the size-selective permeability of the synovium to AuNPs and determine whether this permeability pattern changes in the presence of lipopolysaccharide (LPS) or interleukin-1 $\beta$  (IL-1 $\beta$ ), activators of synovial inflammatory cascades.<sup>19,20</sup> Furthermore, we hypothesized that tissues exposed ex vivo to AuNPs would show a reduction in inflammatory biomarkers compared with control tissues.

\*Correspondence to: Raphael Labens; Email: rlabens@ncsu.edu

Submitted: 01/06/13; Revised: 03/13/13; Accepted: 03/14/13

Citation: Labens R, Lascelles BD, Charlton AN, Ferrero NR, Van Wettère AJ, Xia X-R, et al. Ex vivo effect of gold nanoparticles on porcine synovial membrane.

Tissue Barriers 2013; 1:e24314; <http://dx.doi.org/10.4161/tisb.24314>

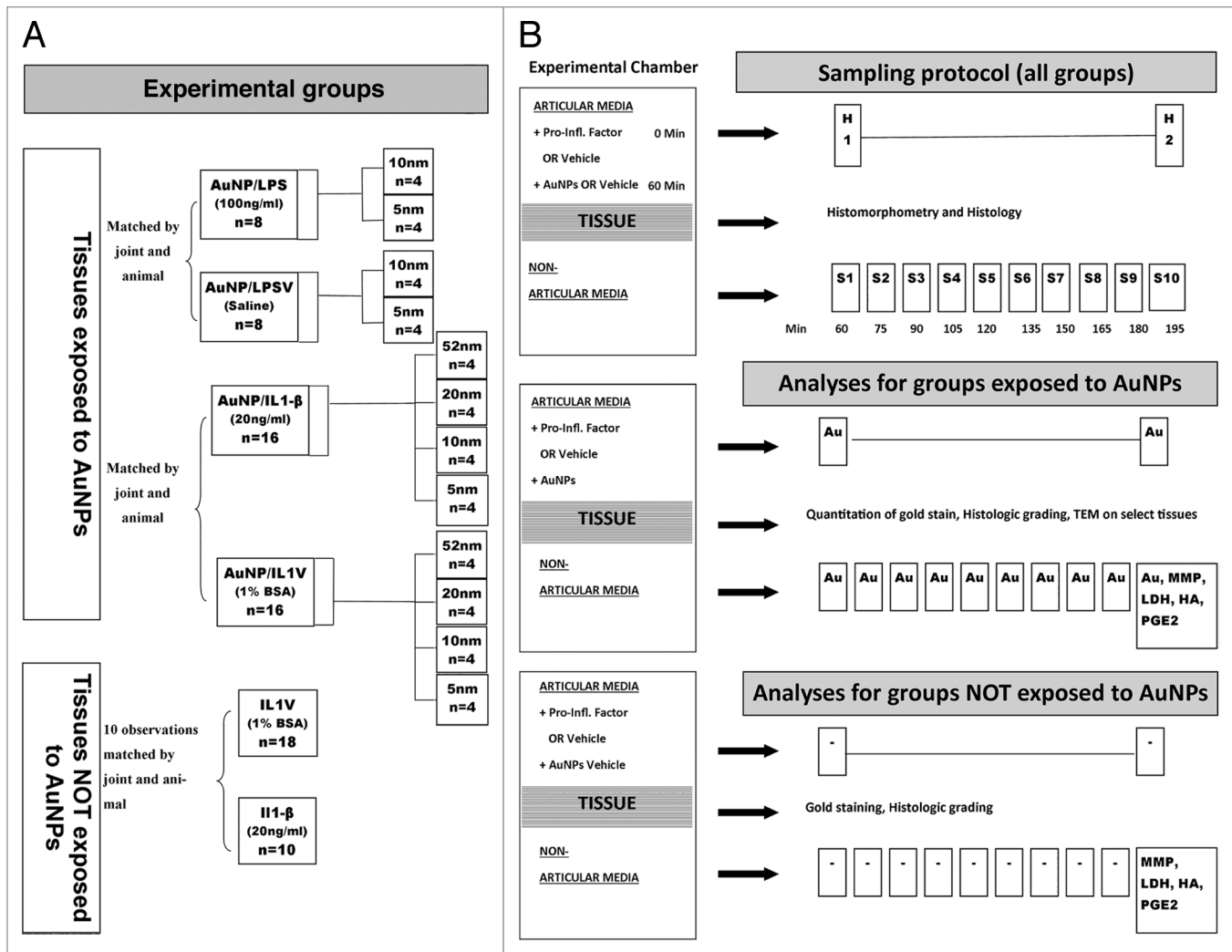


**Figure 1.** Experimental Protocol. (A) Schematic of the experimental groups. (B) Schematic of the experimental procedures (AuNPs, gold nanoparticles; Au, elemental gold; LPS, lipopolysaccharide; LPSV, LPS vehicle; IL-1β, interleukin-1β; IL1V, interleukin-1β vehicle; MMP, matrix metalloproteinase; LDH, lactate dehydrogenase; HA, hyaluronic acid; PGE2, Prostaglandin E2).

## Results

Details on experimental groups and sampling protocol are shown in Figure 1. Tissues exposed to AuNPs received either pro-inflammatory factors (Group AuNP/P-Infl), LPS and IL-1β or their respective vehicle (Group AuNP/V). Groups that were not exposed to AuNPs (control group) received either IL-1β (C/IL-1β) or IL-1β vehicle (C/IL1V).

**AuNP permeation through the synovium.** AuNP permeation through the synovial membrane from the articular to the non-articular chamber compartment was evaluated on the basis of the following measures: The AuNP dose reduction (H1 minus H2 sample concentration), the sequential and cumulative amount of diffusing elemental gold (individual or sum of sample concentrations S1-S10) and the histomorphometric quantitation of gold specific tissue stains. The average AuNP dose (H1 sample) was 7.63 mg/L (range 3.17–18) which at the end of experiments (H2 sample) was reduced to 6.48 mg/L (H2 sample; range

1.11–14.08 mg/L). The average percent reduction in articular AuNP concentration was 23% (SEM 2.63%) for 5 nm, 22.6% (SEM 5.5%) for 10 nm, 3.2% (SEM 2.88%) for 20 nm and 7.2% (SEM 3.73%) for 52 nm AuNPs.

Dry state particle size significantly determined the amount of AuNP diffusion assessed by both histomorphometry and cumulative and sequential elemental gold concentrations ( $p = 0.001$ ). While lesser diffusion was appreciated with greater AuNP size, only comparisons with 5 nm particles reached significance. This illustrated the fact that effective tissue permeation only occurred with the smallest particles (Fig. 2). Next to particle size, the time of sampling also exerted a significant effect in all kinetic data analyses ( $p < 0.001$ ) and this was best appreciated with the use of the 5 nm particles (Fig. 3). As stated previously, this is explained by 5 nm particles permeating through the entire tissues' width, which at the most measured 379.5 μm (SEM 20.9 μm) and at the least 216.3 μm (SEM 17.4 μm).

Examples of the size-dependent permeation of the synovial membrane are demonstrated in **Figure 4**. Transmission electron microscopy was performed as an alternate method to gold staining to validate the presence of AuNPs in tissues, confirming the presence of AuNPs in extra- and intracellular locations. Relatively few particles were observed in the interstitium, presumably due to particle loss during sample preparation. **Figure 5** shows synoviocytes and surrounding interstitium after exposure to 5 nm AuNPs and demonstrates that particles were diffusely distributed throughout the cytoplasm. This observation suggests uptake of the AuNPs through the cytoplasmic membrane independent of endocytosis (**Fig. 5C**). Evidence suggestive of possible endosomal uptake in the form of a membrane bound electron lucent vesicle containing AuNPs (white arrow) and mitochondrial penetration (asterisk) was also seen (**Fig. 5D**). Extracellular locations of larger agglomerates are indicated by black arrows (**Fig. 5A and B**). Nuclear penetration was not observed.

**Effect of pro inflammatory factors on AuNP permeation.** When examining the individual effect of the two pro-inflammatory factors (LPS or IL-1 $\beta$ ) and their vehicle controls (LPSV or IL1V) on synovial permeability, chambers containing IL-1 $\beta$  vehicle (1% bovine serum albumin solution) displayed significantly greater sequential and cumulative AuNP permeation ( $p = 0.001$ ). **Figure 3** illustrates this effect for 5 nm AuNP permeation. When compared with each of their vehicle controls, neither of the two factors exerted a measurable effect on ex vivo synovial AuNP permeation. With respect to the effect of “time,” a significant difference in permeating AuNPs concentrations over baseline values was noted for vehicle and IL-1 $\beta$  use, 105 min and 90 min respectively after dosing ( $p = 0.0119$ ;  $p = 0.0232$ ).

**AuNP effect on biomarkers of inflammation.** To assess the effect of permeating AuNPs on synovial tissues, biomarkers of inflammation (prostaglandin E<sub>2</sub>, PGE<sub>2</sub>; matrix metalloproteinases, MMP), cell integrity (lactate dehydrogenase, LDH) and synoviocyte function (hyaluronic acid, HA) were assessed in non-articular fluid samples. There was

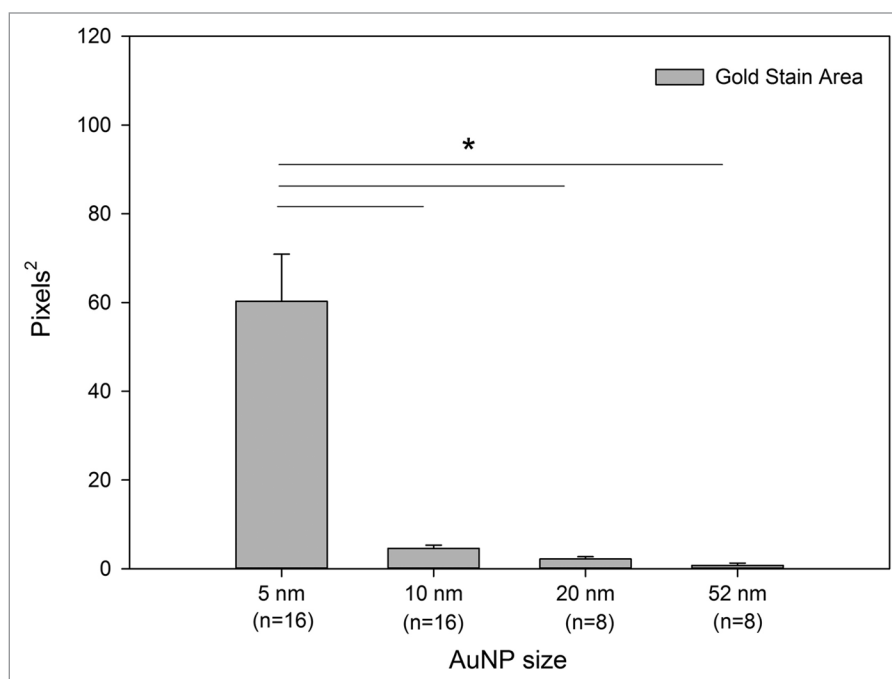


**Figure 2.** Size dependent permeation of the synovial membrane assessed by histomorphometry. Bars represent the average surface area of the gold specific tissue stain (pixel<sup>2</sup>) for each size of gold nanoparticle (AuNP) used (5, 10, 20 and 52 nm). Significance was reached for all comparisons with 5 nm AuNPs ( $p < 0.001$ ). Error bars represent the standard error for the mean.

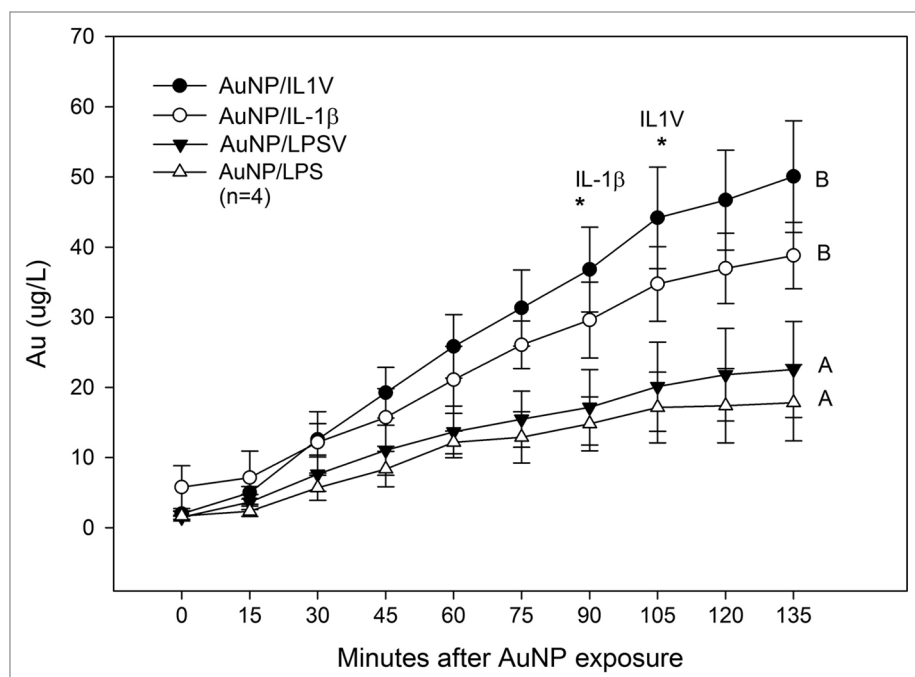


**Figure 3.** Time-dependent permeation of 5 nm gold nanoparticles through the synovial membrane. A significant difference in synovial AuNP permeation was observed between chambers receiving IL-1 $\beta$  vehicle and LPS or LPS vehicle. Significantly different permeation curves ( $p < 0.05$ ) are indicated by different letters. Stars above time points indicate when and for what group sample concentrations were significantly different from baseline values. Error bars represent the standard error for the mean (LPS, lipopolysaccharide; IL-1 $\beta$ , interleukin-1 $\beta$ ; V, vehicle).

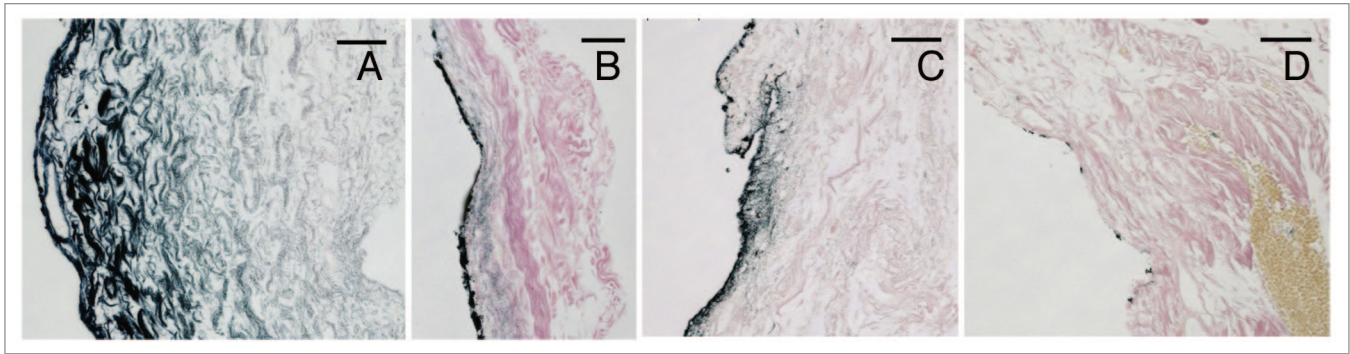


**Figure 4.** Representative images of the size dependent permeation of the synovial membrane. Tissues had been exposed to (A) 5 nm AuNPs, (B) 10 nm AuNPs, (C) 20 nm AuNPs and (D) 52 nm AuNPs prior to gold enhancement. Five nanometer AuNPs can be seen penetrating all tissue layers. Elemental gold appears black (AuNPs, gold nanoparticles; scale bar = 50  $\mu$ m).

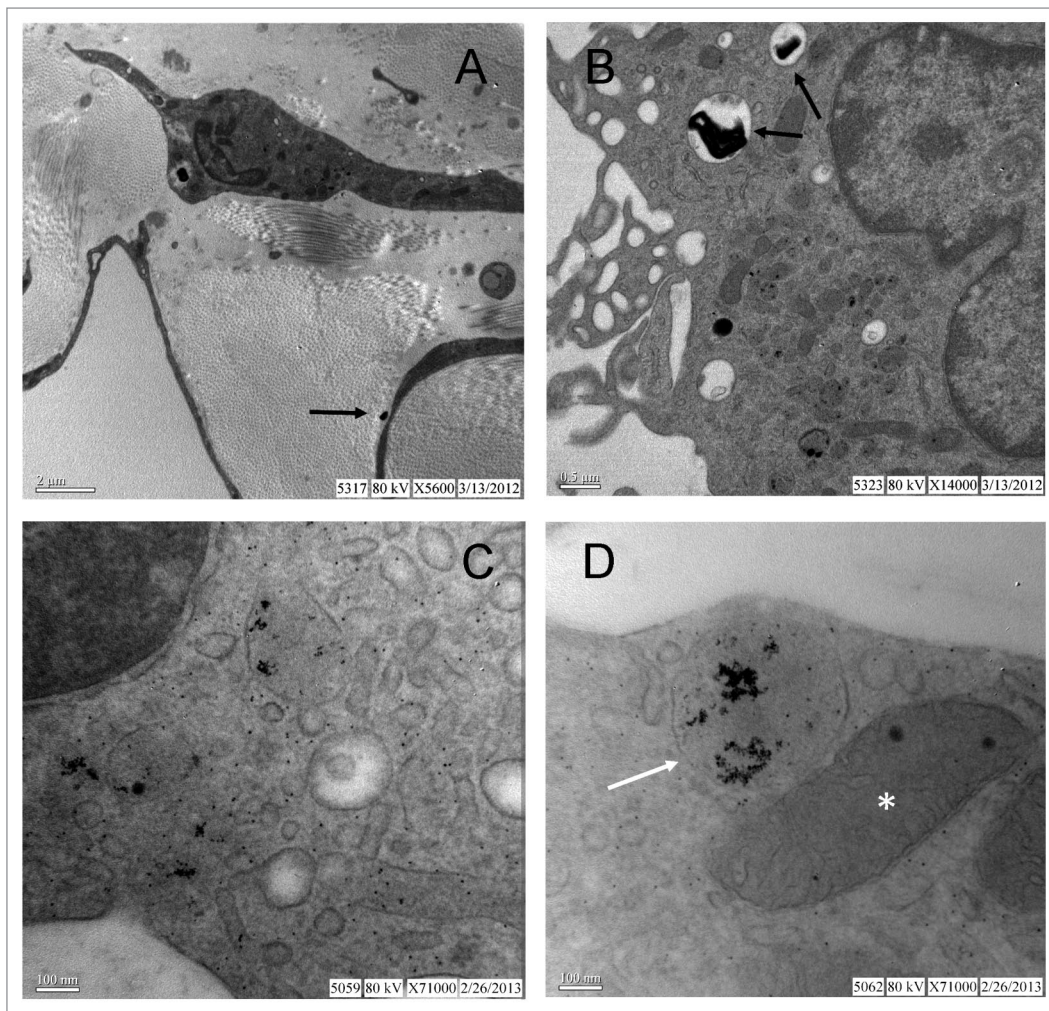


**Figure 5.** Representative transmission electron microscopic images of AuNP localization. By enlarge AuNPs were scattered throughout the cytoplasm and organelles of synoviocytes including the smooth endoplasmic reticulum and mitochondria (C and D). Extracellular location of large particle agglomerates were also appreciated (A and B). Evidence for larger AuNPs agglomerates in endosomes (white arrow) is illustrated in (D).

no significant association of the experimental group with PGE<sub>2</sub> concentrations. Tissues that were exposed to AuNPs showed significantly less MMP ( $p < 0.001$ ) and LDH ( $p < 0.001$ ) activity

and lower HA concentrations ( $p < 0.001$ ). For LDH and HA this significance was limited to individual comparisons with Group C/IL1V (Fig. 6). Positive correlations between biomarkers were

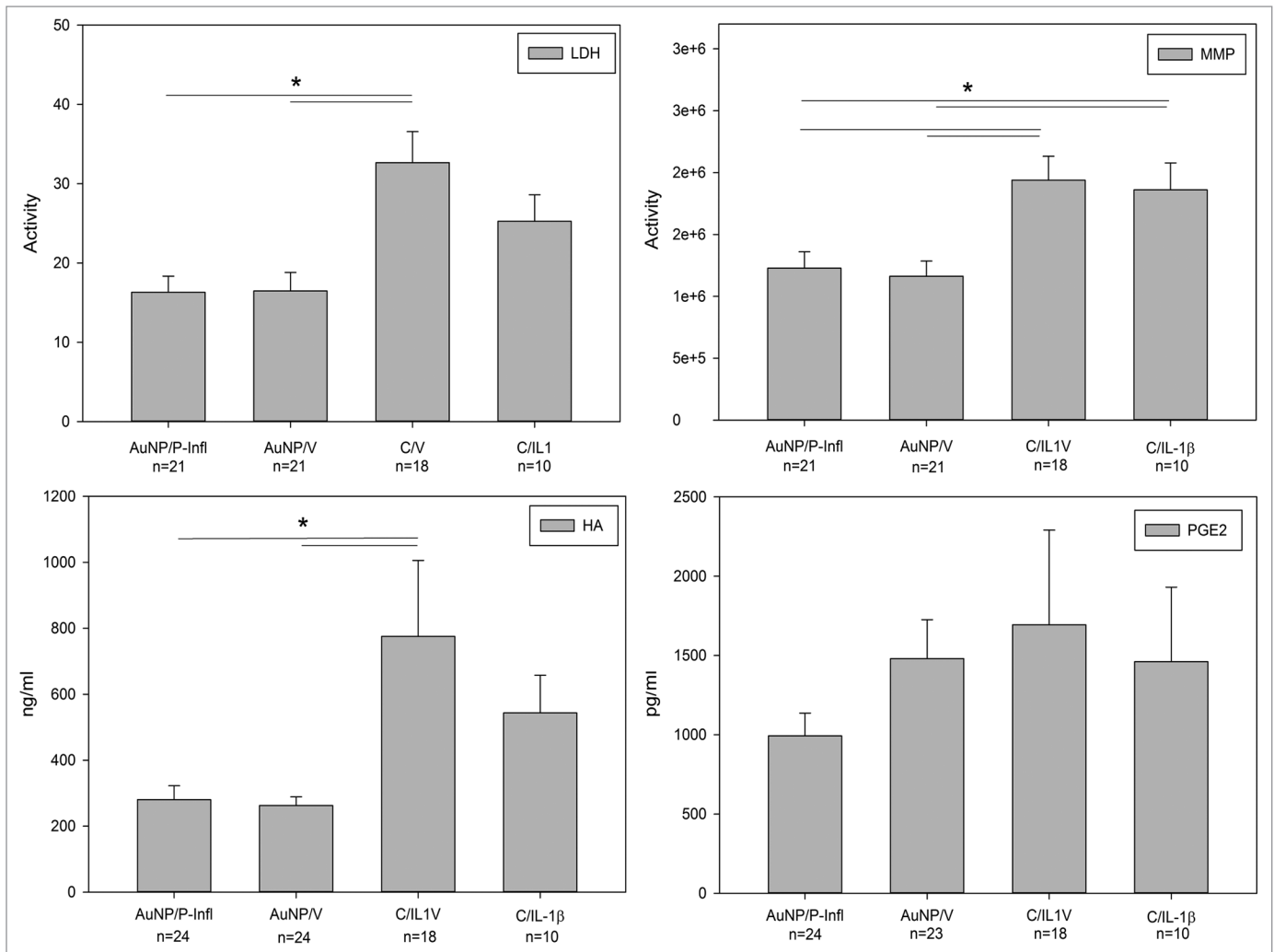


**Figure 6.** Molecular biomarkers by experimental group Group AuNP/P-Infl: Tissues exposed to AuNPs and pro-inflammatory factor Group AuNP/V: Tissues exposed to AuNPs and vehicle; Group C/IL1V: Synovium exposed to Interleukin-1β vehicle only; Group C/IL-1β: Synovium exposed to Interleukin-1β. Error bars represent the standard error for the mean. Bars above group comparisons indicate significance ( $p < 0.05$ ).

limited to LDH with MMP activity (correlation coefficient: 0.386;  $p < 0.001$ ) and HA concentrations (correlation coefficient 0.286;  $p = 0.016$ ). When tissues were exposed to AuNPs and pro-inflammatory factors, LDH, MMP and HA measures were on average 35.4%, 36.4% and 48% of the value when no AuNPs were present; when tissues were exposed to AuNPs alone these values were 49.6%, 35.8% and 66.1% respectively of vehicle treated tissues.

AuNP size had a significant effect on MMP activity ( $p = 0.0046$ ; significant comparisons: 10 vs. 20 nm AuNPs/ $p = 0.0285$ ; 10 vs. 5 nm AuNPs/ $p = 0.0082$ ), LDH activity ( $p < 0.001$ ; 10 vs. 5 nm AuNPs/ $p < 0.001$ ; 20 vs. 5 nm AuNPs/ $p = 0.0226$ ) and HA concentrations ( $p = 0.038$ ; 10 vs. 20 nm AuNPs/ $p = 0.0310$ ). However, these significant differences did not translate into relevant conclusions regarding the effect of particle size on biomarkers.

To evaluate the effect of AuNPs on laboratory techniques and validate results, select biomarker analyses were repeated

with AuNPs added. PGE<sub>2</sub> and HA concentration standards with AuNPs added resulted in an average increase equal to 56 and 4.5% of the value when AuNPs were not present (corrected for dilution). MMP and LDH activity decreased by 22.7 and 0.77%.

**Effect of pro-inflammatory factors on biomarkers of inflammation.** No significant difference in biomarker levels was observed between tissues exposed to pro-inflammatory factors and their controls (Fig. 6).

**Histopathology of the synovial membrane.** Histologic changes were assessed on the basis of a semi-quantitative grading scale for which examples are shown in Figure 7. Notable ex vivo changes were limited to synovial ulcerations. Only one of the synovial membrane samples was categorized as edematous (Grade 2). When Group C/IL1V was considered the reference standard, the proportion of histologic grades differed significantly among the three remaining groups with 63% in Group AuNP/P-Infl, 59% in Group AuNP/V and 0% in Group C/IL-1β showing ulceration greater than 5% of the sections' surface

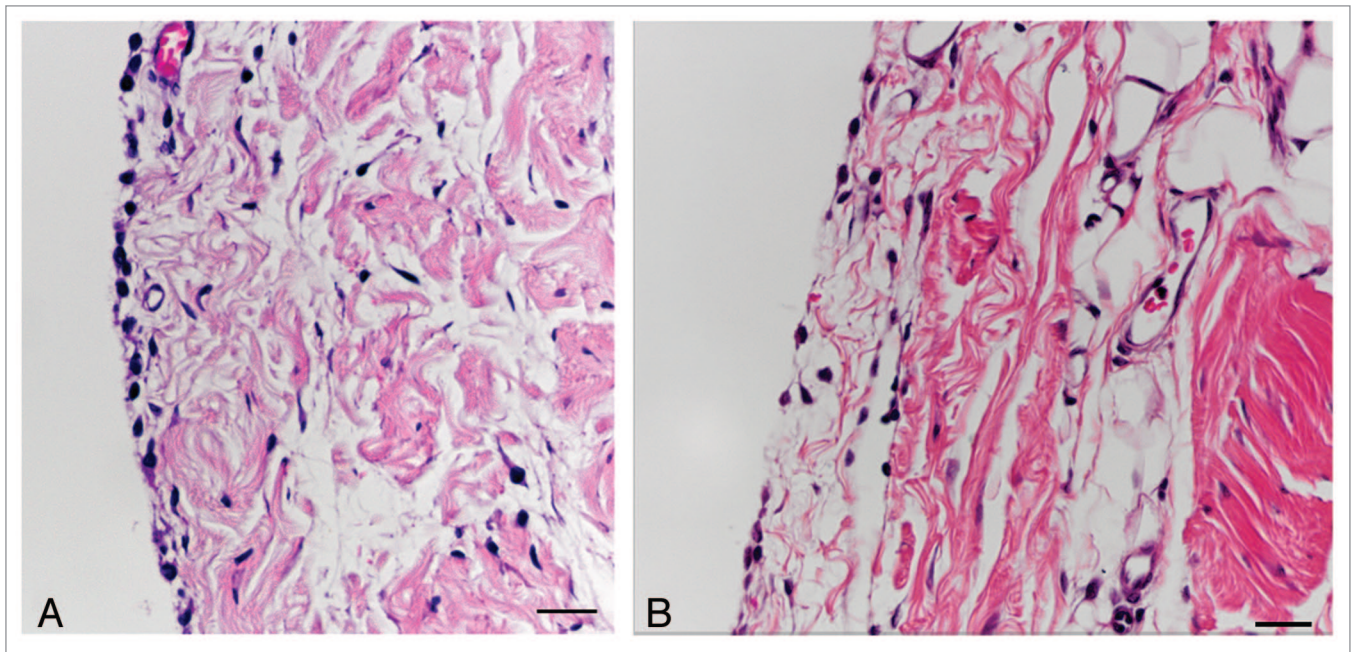


**Figure 7.** Representation of synovial ulceration. The degree of synovial ulceration was graded based on the estimated percentage of synovium missing over the length of the sample evaluated. (A) shows a representation of the synovial lining at 60× magnification that was considered normal; a continuous lining of synovial cell is present. (B) Represents tissue at the same magnification with ulceration of the synovium; a discontinuous lining of synovial cell is observed over the subsynovial connective tissue (bar = 30 µm).

( $p = 0.0087$ ). However in statistical analyses the histologic grade had no effect on biomarker levels.

**Particle stability in the fluid environment.** The hydrodynamic size of AuNPs in components of articular fluid media was assessed to interpret the particles' ability to permeate tissues in chamber experiments in the context of physical and functional size. When AuNPs were added to articular media, an increase in hydrodynamic size was noted which was attributed to particle agglomeration. This effect was most pronounced for 5 nm particles and when LPS was added to the media (Table 1). Hydrodynamic sizes of AuNPs in IL-1 $\beta$  vehicle containing fluids remained relatively unchanged confirming a stabilizing effect of the 1% bovine serum albumin solution and supporting findings shown in Figure 3.

## Discussion

Confirming the authors' hypothesis, samples of synovial membrane were successfully mounted in the Ussing chamber and demonstrated size selective permeability to AuNPs both on inductively coupled plasma mass spectrometry and histomorphometry. However, effective permeation of tissue samples measured with mass spectrometry was only observed using AuNPs of 5 nm dry state size. Previous in vivo work in rabbit stifles suggests that effective matrix pore size ranges between 66 and 118 nm allowing smaller molecules to leave the joint environment freely.<sup>21</sup> Our observation that 52 nm particles were unable to breach the subintima may be in line with these findings but the propensity of bare AuNPs to agglomerate and result in greater hydrodynamic size may make this conclusion less relevant (Table 1).<sup>22</sup> In

contrast to our expectations, ex vivo exposure to pro-inflammatory factors did not significantly affect biomarker levels. This is likely the result of the inherent activation associated with tissue collection that cannot be surpassed by further ex vivo stimulation. A similar phenomenon has been observed when using porcine gastrointestinal tissues, which required pre-treatment with a cyclooxygenase inhibitor to study subsequent prostaglandin-dependent outcome measures.<sup>23</sup> The porcine and murine IL-1 $\beta$  cDNA sequence show 74% homologies with the human form<sup>24</sup> and use of human recombinant IL-1 $\beta$  has been effective in tissues from both species.<sup>25-30</sup> Nevertheless, heterology between human and porcine cytokines should also be considered in the absence of a significant IL-1 $\beta$  effect. Concerning the selection of IL-1 $\beta$  as the pro-inflammatory factor, the role of this cytokine in joint disease has been well documented.<sup>20,31-35</sup> The dose applied was chosen taking previous in vitro<sup>36,37</sup> and in vivo heterologous use of recombinant human IL-1 $\beta$  into consideration and adjusting for the typical fluid volume in injected joints vs. the Ussing chamber system.<sup>38,39</sup> Despite these considerations the dose selection may have been inappropriate. The authors are aware of these specific limitations and future investigations will include the use of recombinant porcine IL-1 $\beta$  and dose-response experiments to further elucidate the pro-inflammatory potential of this cytokine in an ex vivo model of synovial tissue.

A previous in vivo study on rabbit synovium illustrated a loss in barrier function and increase in diffusion of hyaluronic acid molecules with enzymatic degradation of extracellular matrix proteins.<sup>40</sup> In our study, use of IL-1 $\beta$  did not initiate a similar effect on AuNP permeation. This may have been caused in part by factors described in the preceding section. However, inability

**Table 1.** Hydrodynamic size of gold nanoparticles (AuNPs) in different fluid environments

Dry state size (nm)	In distilled water (nm)	In simulated chamber fluid (nm)	In simulated chamber fluid + IL1 $\beta$ (nm)	In simulated chamber fluid + IL1 $\beta$ -C (nm)	In simulated chamber fluid + LPS (nm)
5	30	700	157	72	790
10	24	432	98	78	495
20	25	345	69	62	489
52	64	284	88	84	293

IL1 $\beta$ -C, interleukin-1 $\beta$  vehicle; LPS, Lipopolysaccharide.

to recruit vascular effector cells promoting tissue inflammation and degradation in an ex vivo model may also be involved. In this study LPS exposure appeared to reduce synovial permeability to AuNPs compared with IL-1 $\beta$  use. However this effect was predominantly driven by the absence of IL-1 $\beta$  vehicle, leading to particle agglomeration and reduced permeation.

Nanoparticles show complex behavior in biological systems based on their composition, size, shape, surface charge and chemistry.<sup>41</sup> Derived from the intensity of scattered light the hydrodynamic size describes the dimension of a spherical particle in fluid media surrounded by the solvation layer.<sup>41</sup> It provides information on the particle's stability or agglomeration state which is dependent on surface charge and ultimately the particle's interactions with different fluid components (ions and proteins).<sup>42</sup> From the hydrodynamic sizing of AuNPs in different chamber fluid components it can be concluded that particles agglomerated in saline solution and that this was increased with the presence of LPS and decreased with the use of 1% bovine serum albumin solution. These effects have in part been reported previously<sup>22,43,44</sup> and are supported by our conclusion that presence of IL-1 $\beta$  vehicle increased AuNP permeation.

From the results it may be further concluded that AuNPs promoted cell viability (reduced LDH activity),<sup>45</sup> reduced MMP activity and HA concentrations while exerting no significant effect on PGE<sub>2</sub> concentrations. These findings need to be interpreted with caution as evidenced by the limited investigation of the AuNP effect on performed assays. Nanoparticles have the ability to interfere with biological assays based on adsorbance of reagents or reporter dyes, optical absorbance and interaction with the primary analyte.<sup>45-47</sup> Although LDH assay performance was not affected by AuNPs in our study, this potential bias has been demonstrated for other nanoparticles.<sup>48</sup> In contrast, PGE<sub>2</sub> assays overestimated true concentrations by an average of 56%. Prostaglandin immunoassays are based on the competitive antibody binding of sample PGE<sub>2</sub> and acetylcholinesterase bound PGE<sub>2</sub> molecules. Enzyme driven conversion of Ellman's reagent results in a yellow color reaction that is inversely proportional to sample PGE<sub>2</sub> concentrations. Considering the great affinity of nanoparticles to acetylcholinesterase, overestimation of the actual PGE<sub>2</sub> content was likely caused by AuNP-dependent enzyme inhibition.<sup>49</sup> Assuming that PGE<sub>2</sub> concentrations are in fact lower than reported, they may be in line with the observed trend that AuNPs reduce biomarkers of inflammation.

Based on the absence of a marked nanoparticle effect on HA assay performance, the conclusion that AuNPs reduced HA concentrations is likely valid. IL-1 $\beta$  stimulation has the potential to

increase HA production via activation of synthases located on the inner surface of cell membranes.<sup>50</sup> In this process synthases continuously assemble disaccharide molecules to form longer chains, extruding from the cell surface into the extracellular space.<sup>51</sup> Possible explanations for the observed reduction in HA levels may include AuNP dependent inhibition of synthases or IL-1 $\beta$  adsorption.<sup>52</sup> Alternatively, low concurrent LDH activity levels may be indicative of fewer HA chains being dissociated from the cell surface due to greater membrane stability when AuNPs were present. However, this potential explanation is contradicted by the histological finding that exposure to AuNPs resulted in greater synovial ulceration.

As alluded to previously, nanoparticles have the ability to interfere with cellular function based on their reactivity and binding of key proteins. This reportedly includes vascular endothelial growth factor and IL-1 $\beta$ .<sup>10,52,53</sup> Exposure of LPS-activated macrophages, a cell line similar to synoviocytes (Type A), to polyethylene glycol coated AuNPs suggests that direct effects also include inhibition of inducible nitric oxide synthase expression.<sup>54</sup> Besides these effects, administration of gold particles may lead to gold ion elution<sup>9,55-58</sup> which in turn could result in therapeutic effects comparable to those of other gold-based pharmaceuticals. Most importantly these effects could include inhibition of NF-kappa B<sup>59-61</sup> and downregulation of the p38 MAPK pathway.<sup>62</sup> In the present experiments, synovial tissue samples were maintained in Ussing chambers for 195 min. From other applications it is known that treatment-induced changes in PGE<sub>2</sub> concentrations occur within this experimental time frame.<sup>63,64</sup> Whether this time is sufficient for the observed changes in HA or MMP levels to develop remains to be determined but causes that involve downstream interference at the level of enzyme function rather than the signaling pathway may be more plausible. In fact, significant in vitro IL-1 $\beta$  activation of intracellular signaling pathways to increase MMP synthesis was detected one hour post stimulation.<sup>65</sup> Recent evidence obtained in vivo demonstrated a significant change in MMP and PGE<sub>2</sub> concentrations 4 h post IL-1 $\beta$  exposure.<sup>66</sup> Taken together this may suggest that our experimental time frame may have been too short to illustrate significant upstream effects on biomarker concentrations.

Given that in our experiments, ability to permeate tissues was not associated with a greater effect on biomarkers, in vivo use of larger AuNPs may be preferred in an attempt to minimize systemic absorption and potential toxic side effects.<sup>67-69</sup> Support for this conclusion may be found in the only other study available for comparison, which demonstrated that a positive in vivo treatment

effect of AuNPs was also not dependent on particle size.<sup>11</sup> Interestingly, next to other dramatic positive effects of AuNPs in this study, a reduction in cell necrosis was also reported, further validating our observation of reduced LDH activity.

Regarding systemic side effects, murine studies suggest that after intravenous administration biodistribution of AuNPs is in part size dependent and that particles predominantly accumulate in the liver, lung and spleen but can also be found in the brain if smaller than 50 nm.<sup>67</sup> Gene expression profiling of liver tissue 30 min after intravenous administration of polyethylene glycol-coated AuNPs (4.3 mg/kg) showed that less than 0.5% of all genes were specifically expressed and that these genes were responsible for apoptosis, cell cycle, inflammation and metabolic processes.<sup>70</sup> Seven days after intravenous administration and depending on the dose administered (0.17 to 4.3 mg/kg) an average of 2.6 to 8.5% of liver cells underwent apoptosis compared with 0.4% in controls.<sup>71</sup> Collectively, these studies demonstrate the potential for systemic side effects following AuNP administration. While doses in our investigation should be considered high in light of the amount of tissue exposed (0.04 mg/1.14 cm<sup>2</sup>) they are low in the context of total body exposure and potential systemic biodistribution (0.00148 mg/kg; by approximation).

In summary, the results reported herein suggest that intra-articular application of 5 nm AuNPs (dry state size) leads to particle permeation through the joint capsule, facilitating systemic bioavailability. Based on this and previous work it is further expected that nanoparticles leave the joint cavity in a size dependent manner either unassisted or within cells and accumulate in the reticuloendothelial system.<sup>21,72</sup> Beyond a yet to be determined size but likely in the range of 50 nm, we anticipate AuNPs to be largely retained within the synovial environment. We consider this to be a relevant characteristic in light of the potential use of AuNPs as drug carriers or primary therapeutics and the potential for systemic side effects. In this investigation, we associate AuNP administration with a significant reduction in inflammatory biomarkers except PGE<sub>2</sub>, but limitations of this study have to be considered. Future studies will seek to validate our ex vivo experiments by including more analytical time points, in vivo exposure to homologous cytokines and AuNP while still collecting ex vivo outcome data. This approach will minimize potential bias of AuNPs on assays, increase the stimulatory effect of pro-inflammatory cytokines and allow time dependent assessment of biomarkers.

## Materials and Methods

**Tissue acquisition.** Synovial membrane samples were obtained from pigs sacrificed at the authors' institution for unrelated research or teaching purposes approved by the Institutional Animal Care and Use Committee. Animals weighed between 22 and 31 kg and were euthanized with an intravenous barbiturate overdose. In each animal synovial membrane was harvested from one femoropatellar joint. To do so the patella was released from its proximal and distal attachments and bisected to open the joint in a "barn-door" fashion resulting in two areas of preserved synovial membrane located between each femoral trochlear ridge and

hemi-patella. Continuous tissue samples were obtained by blunt dissection undermining the synovial membrane in that area. Within one hour, samples were transported to the laboratory in oxygenated (95% O<sub>2</sub> and 5% CO<sub>2</sub>) Ringer's solution (323.9 mOsm/l; Na<sup>+</sup> 154.1, K<sup>+</sup> 6.3, Cl<sup>-</sup> 137.3, H<sub>2</sub>PO<sub>4</sub><sup>-</sup> 0.3, Ca<sup>2+</sup> 1.2, Mg<sup>2+</sup> 0.7, HCO<sub>3</sub><sup>-</sup> 24 mmol/l) at room temperature and mounted in Ussing chambers with a 1.14 cm<sup>2</sup> aperture.

**Ussing chambers.** Synovial tissue samples were bathed on the intima (articular) and subintima (non-articular) side with 5 ml of oxygenated Ringer's solution maintained at 37°C via water-jacked reservoirs. Glucose was added to the non-articular side and mannitol to the articular side (10 mmol/L) of the Ussing chamber for oncotic balance. At time "0," the articular side of the chambers were either treated with 100 ng/ml of LPS in Ringer's solution (from *E. coli* 0111:B4, L4130, Sigma-Aldrich), 20 ng/ml of human recombinant IL-1β (SRP3083, Sigma-Aldrich) suspended in a 1% solution of bovine serum albumin or vehicle control solution (Ringer's solution or bovine serum albumin solution). After one hour the articular fluid compartments were either dosed with an unconjugated spherical gold nanoparticle (AuNP) solution (Nanopartz, Accurate Spherical Gold Nanoparticles, mean particle sizes 5, 10, 20 and 52 nm) that was previously sonicated for one minute or with a saline control. Subsequently the bathing fluid of the non-articular side was sampled (1 ml) and every 15 min thereafter until completion of the experiment (S1–S10, 60–195 min post tissue mounting). Fluid of the articular compartment was sampled twice (0.5 ml at time "60" (H1) and "195" (H2)). Non-articular reservoir fluids were replenished using the Ringer's and glucose solution. All fluid samples were immediately frozen in liquid nitrogen and stored at -80°C until they were thawed on ice, vortexed and further analyzed.

**AuNP hydrodynamic size.** Samples of the nanoparticle dosing solution were mixed with the simulated articular fluid media or distilled water (1:4), sonicated for 5 min and the hydrodynamic size was assessed in a 100 μl sample using dynamic light scattering methods (ZetaSizer, Malvern Instruments). Size measurements were averaged across 60 repeated measurements obtained in triplicate runs of the same sample.

**AuNP quantitation.** Elemental gold concentration in articular and non-articular fluid samples was determined using inductively coupled plasma mass spectrometry (Varian 820) with an estimated detection limit of 0.1 μg/L. Gold concentrations of samples (S1–S10) were summed to give a cumulative amount of permeating AuNPs for each chamber.

**Prostaglandin E<sub>2</sub> (PGE<sub>2</sub>) quantitation.** A competitive ELISA kit (Cayman Chemical, Item No 514010) was used with samples analyzed in triplicate. Outliers that resulted in a coefficient of variance greater than 30% were excluded from the analysis.

**Hyaluronic acid (HA) quantitation.** An enzyme linked binding protein assay was used to determine HA concentrations (ng/ml) of articular fluid samples in duplicate analyses (Corgenix Inc., 029-001).

The effect of gold particles on the PGE<sub>2</sub> and HA assays was determined by running the standards (S4 and medium molecular weight HA) with and without AuNPs added. This was performed in duplicate for each nanoparticle size.

**Matrix metalloproteinase (MMP) activity.** Using a previously described technique<sup>73</sup> MMP activity (MMP 2, 3, 7, 9, 12 and 13) was determined using an activatable near infrared (NIR) fluorescent probe added to articular fluid samples in a 96-well plate (MMPsense 750 FAST, PerkinElmer) and a NIR fluorescence reader (Ivis Lumina II, PerkinElmer).

The effect of AuNPs on MMP measurements was investigated by repeated analysis of three fluid samples with and without 5 nm AuNPs added.

**Lactate dehydrogenase (LDH) activity.** A toxicology assay kit (TOX7, Sigma-Aldrich) was used to determine the enzyme's activity in articular fluid samples based on a stoichiometric colorimetric reaction measured at a wavelength of 490 nm. Samples of Group C/IL1V were rerun in duplicate with AuNPs (all sizes) added.

**Tissue processing.** Tissue samples were fixed using MacDowell's and Trump's 4F:1G solution, embedded in paraffin and three cross sections per synovial membrane were acquired. One section was stained with hematoxylin and eosin (H&E) only, two underwent autometallographic gold enhancement for 20 min (Goldenhance-LM/Blot, Nanoprobes) and one of these was later also stained with H&E. Tissue samples were also embedded in Spurr resin followed by ultrathin sectioning for transmission electron microscopy.

**Histomorphometry.** Slides were anonymized, randomized and for each synovium sample, the entire length of the sample was photographed at 10× and 40× using an Olympus DP 25 digital microscope camera with the CellSens digital imaging software mounted on an Olympus BH 41 microscope (Olympus Corporation, Tokyo, Japan). Using Adobe Photoshop CS4 (PhotoshopCS4; Adobe Systems) and via batch processing, 40× images were converted to 6,000 × 4,500 pixels (100 pixels/cm) and to black and white in order to highlight the gold particle. The batch processing procedure allowed the same setting to be applied to all images in a given data set. The best setting was determined empirically by testing images with the lowest and highest amount of gold particles. Finally, images were thresholded in the "intermodes" setting and the area fraction covered with the gold particles, expressed as a percentage of the picture surface area, was measured using an open source image analysis system (ImageJ, NIH). 10× images were used to measure the

tissue's maximum and minimum width in each image and measurements were subsequently averaged to give an average maximum and minimum width for each sample.

**Histology.** A board certified pathologist, blinded to the identity of each slide graded the degree of synovial ulceration (0 = no ulcer or less than 5%; 1 = up to 25%; 2 = up to 50%; 3 = up to 75% and 4 = more than 75% of the synovial surface) and sub-synovial connective tissue edema (0 = no edema; 1 = mild; 2 = moderate; 3 = severe). Tissue samples that were neither stimulated nor had gold exposure (Group C/IL1V) were used as a reference standard.

**Transmission electron microscopy.** Synovial samples were fixed in 4F:1G, dehydrated in a graded series of ethanol and embedded in Spurr resin.<sup>74</sup> Semithin sections, 0.5 μm thick, stained with 1% toluidine blue in 1% sodium borate, were examined under a light microscope. Ultrathin sections, 90 nm thick, of appropriate blocks were examined with a FEI/Philips EM 208S transmission electron microscope. Only tissue samples exposed to 5 nm AuNPs were examined.

**Statistical analyses.** A Fisher's exact test was used to compare proportions of histologic grades by experimental group (AuNP/P-Infl, AuNP/V, C/IL-1β). Using the mixed procedure (SAS 9.2, SAS Institute Inc.) the significance of individual independent variables, AuNP presence (yes or no), AuNP size (5, 10, 20, 52 nm), use of pro-inflammatory factor (yes or no), type of pro-inflammatory factor (IL-1β or LPS), experimental group (AuNP/P-Infl, AuNP/V, C/IL1V, C/IL-1β), was determined. Variables showing co-linearity were analyzed separately. Models were fitted separately for each biomarker (PGE<sub>2</sub>, MMP, LDH, gold stain area, cumulative elemental gold concentration). Relevant comparisons were performed using an LSMEANS statement and the Tukey adjustment for multiple testing. Relationships between dependent variables were investigated using Pearson correlations.

Kinetic data obtained with mass spectroscopic gold determinations were analyzed using repeated measures ANOVA with "time" as the repeated variable. For all statistical analyses the critical p value was set at 0.05.

#### Disclosure of Potential Conflicts of Interest

No potential conflict of interest was disclosed.

#### References

1. Higby GJ. Gold in medicine: a review of its use in the West before 1900. *Gold Bull* 1982; 15:130-40; PMID:11614517; <http://dx.doi.org/10.1007/BF03214618>.
2. Rau R. Have traditional DMARDs had their day? Effectiveness of parenteral gold compared to biologic agents. *Clin Rheumatol* 2005; 24:189-202; PMID:15940552; <http://dx.doi.org/10.1007/s10067-004-0869-8>.
3. Hamilton J, McInnes IB, Thomson EA, Porter D, Hunter JA, Madhok R, et al. Comparative study of intramuscular gold and methotrexate in a rheumatoid arthritis population from a socially deprived area. *Ann Rheum Dis* 2001; 60:566-72; PMID:11350844; <http://dx.doi.org/10.1136/ard.60.6.566>.
4. Lehman AJ, Esdaile JM, Klinkhoff AV, Grant E, Fitzgerald A, Canvin J; METGO Study Group. A 48-week, randomized, double-blind, double-observer, placebo-controlled multicenter trial of combination methotrexate and intramuscular gold therapy in rheumatoid arthritis: results of the METGO study. *Arthritis Rheum* 2005; 52:1360-70; PMID:15880810; <http://dx.doi.org/10.1002/art.21018>.
5. Smolen JS, Landewé R, Breedveld FC, Dougados M, Emery P, Gaujoux-Viala C, et al. EULAR recommendations for the management of rheumatoid arthritis with synthetic and biological disease-modifying antirheumatic drugs. *Ann Rheum Dis* 2010; 69:964-75; PMID:20444750; <http://dx.doi.org/10.1136/ard.2009.126532>.
6. Sander O, Herborn G, Bock E, Rau R. Prospective six year follow up of patients withdrawn from a randomised study comparing parenteral gold salt and methotrexate. *Ann Rheum Dis* 1999; 58:281-7; PMID:10225812; <http://dx.doi.org/10.1136/ard.58.5.281>.
7. Nejrup K, Olivarius NdeF, Jacobsen JL, Siersma V. Randomised controlled trial of extraarticular gold bead implantation for treatment of knee osteoarthritis: a pilot study. *Clin Rheumatol* 2008; 27:1363-9; PMID:18500437; <http://dx.doi.org/10.1007/s10067-008-0918-9>.
8. Jaeger GT, Larsen S, Söli N, Moe L. Double-blind, placebo-controlled trial of the pain-relieving effects of the implantation of gold beads into dogs with hip dysplasia. *Vet Rec* 2006; 158:722-6; PMID:16731702; <http://dx.doi.org/10.1136/vr.158.21.722>.
9. Danscher G. In vivo liberation of gold ions from gold implants. Autometallographic tracing of gold in cells adjacent to metallic gold. *Histochem Cell Biol* 2002; 117:447-52; PMID:12029492; <http://dx.doi.org/10.1007/s00418-002-0400-8>.
10. Tsai CY, Shiau AL, Chen SY, Chen YH, Cheng PC, Chang MY, et al. Amelioration of collagen-induced arthritis in rats by nanogold. *Arthritis Rheum* 2007; 56:544-54; PMID:17265489; <http://dx.doi.org/10.1002/art.22401>.

11. Leonavičienė L, Kirdaitė G, Bradūnaitė R, Vaitkienė D, Vasiliauskas A, Zabulytė D, et al. Effect of gold nanoparticles in the treatment of established collagen arthritis in rats. *Medicina (Kaunas)* 2012; 48:91-101; PMID:22491387.
12. Dykman LA, Khlebtsov NG. Gold nanoparticles in biology and medicine: recent advances and prospects. *Acta Naturae* 2011; 3:34-55; PMID:22649683.
13. Edwards SH. Intra-articular drug delivery: the challenge to extend drug residence time within the joint. *Vet J* 2011; 190:15-21; PMID:20947396; <http://dx.doi.org/10.1016/j.tvjl.2010.09.019>.
14. Butoescu N, Jordan O, Doelker E. Intra-articular drug delivery systems for the treatment of rheumatic diseases: a review of the factors influencing their performance. *Eur J Pharm Biopharm* 2009; 73:205-18; PMID:19545624; <http://dx.doi.org/10.1016/j.ejpb.2009.06.009>.
15. Squier CA, Mantz MJ, Schlievert PM, Davis CC. Porcine vagina ex vivo as a model for studying permeability and pathogenesis in mucosa. *J Pharm Sci* 2008; 97:9-21; PMID:17721937; <http://dx.doi.org/10.1002/jps.21077>.
16. Blikslager AT, Moeser AJ, Gookin JL, Jones SL, Odle J. Restoration of barrier function in injured intestinal mucosa. *Physiol Rev* 2007; 87:545-64; PMID:17429041; <http://dx.doi.org/10.1152/physrev.00012.2006>.
17. Walsh AJ, Poole KM, Duvall CL, Skala MC. Ex vivo optical metabolic measurements from cultured tissue reflect in vivo tissue status. *J Biomed Opt* 2012; 17:116015; PMID:23117810; <http://dx.doi.org/10.1117/1.JBO.17.11.116015>.
18. Davies J. Potential Advantages of Using Biomimetic Alternatives. In: Davies J, ed. *Replacing Animal Models: A practical Guide to Creating and Using Culture-based Biomimetic Alternatives*: John Wiley & Sons, 2012.
19. Morton AJ, Campbell NB, Gayle JM, Redding WR, Blikslager AT. Preferential and non-selective cyclooxygenase inhibitors reduce inflammation during lipopolysaccharide-induced synovitis. *Res Vet Sci* 2005; 78:189-92; PMID:15563928; <http://dx.doi.org/10.1016/j.rvsc.2004.07.006>.
20. Sutton S, Clutterbuck A, Harris P, Gent T, Freeman S, Foster N, et al. The contribution of the synovium, synovial derived inflammatory cytokines and neuropeptides to the pathogenesis of osteoarthritis. *Vet J* 2009; 179:10-24; PMID:17911037; <http://dx.doi.org/10.1016/j.tvjl.2007.08.013>.
21. Sabaratnam S, Arunan V, Coleman PJ, Mason RM, Levick JR. Size selectivity of hyaluronan molecular sieving by extracellular matrix in rabbit synovial joints. *J Physiol* 2005; 567:569-81; PMID:15961430; <http://dx.doi.org/10.1113/jphysiol.2005.088906>.
22. Bergen JM, von Recum HA, Goodman TT, Massey AP, Pun SH. Gold nanoparticles as a versatile platform for optimizing physicochemical parameters for targeted drug delivery. *Macromol Biosci* 2006; 6:506-16; PMID:16921538; <http://dx.doi.org/10.1002/mabi.200600075>.
23. Blikslager AT, Roberts MC, Argenzio RA. Prostaglandin-induced recovery of barrier function in porcine ileum is triggered by chloride secretion. *Am J Physiol* 1999; 276:G28-36; PMID:9886975.
24. Huether MJ, Lin G, Smith DM, Murtaugh MP, Molitor TW. Cloning, sequencing and regulation of an mRNA encoding porcine interleukin-1 beta. *Gene* 1993; 129:285-9; PMID:8325511; [http://dx.doi.org/10.1016/0378-1119\(93\)90281-7](http://dx.doi.org/10.1016/0378-1119(93)90281-7).
25. Pecchi E, Priam S, Mladenovic Z, Gosset M, Saurel AS, Aguilar L, et al. A potential role of chondroitin sulfate on bone in osteoarthritis: inhibition of prostaglandin E and matrix metalloproteinases synthesis in interleukin-1 $\beta$ -stimulated osteoblasts. *Osteoarthritis Cartilage* 2012; 20:127-35; PMID:22179028; <http://dx.doi.org/10.1016/j.joca.2011.12.002>.
26. Chandrasekhar S, Harvey AK, Hruby PS. Intra-articular administration of interleukin-1 causes prolonged suppression of cartilage proteoglycan synthesis in rats. *Matrix* 1992; 12:1-10; PMID:1560785; [http://dx.doi.org/10.1016/S0934-8832\(11\)80099-5](http://dx.doi.org/10.1016/S0934-8832(11)80099-5).
27. Goodstone NJ, Hardingham TE. Tumour necrosis factor alpha stimulates nitric oxide production more potently than interleukin-1beta in porcine articular chondrocytes. *Rheumatology (Oxford)* 2002; 41:883-91; PMID:12154205; <http://dx.doi.org/10.1093/rheumatology/41.8.883>.
28. Shimokawa H, Ito A, Fukumoto Y, Kadokami T, Nakaike R, Sakata M, et al. Chronic treatment with interleukin-1 beta induces coronary intimal lesions and vasospastic responses in pigs in vivo. The role of platelet-derived growth factor. *J Clin Invest* 1996; 97:769-76; PMID:8609234; <http://dx.doi.org/10.1172/JCI118476>.
29. Bai LJ, Tuch BE, Hering B, Simpson AM. Fetal pig beta cells are resistant to the toxic effects of human cytokines. *Transplantation* 2002; 73:714-22; PMID:11907416; <http://dx.doi.org/10.1097/00007890-200203150-00010>.
30. Jana B, Kozłowska A, Andronowska A, Jedlińska-Krakowska M. The effect of tumor necrosis factor-alpha (TNF-alpha), interleukin (IL)-1 beta and IL-6 on chorioamnion secretion of prostaglandins (PG)F 2 alpha and E2 in pigs. *Reprod Biol* 2008; 8:57-68; PMID:18432307; [http://dx.doi.org/10.1016/S1642-431X\(12\)60004-7](http://dx.doi.org/10.1016/S1642-431X(12)60004-7).
31. Kojima F, Kato S, Kawai S. Prostaglandin E synthase in the pathophysiology of arthritis. *Fundam Clin Pharmacol* 2005; 19:255-61; PMID:15910650; <http://dx.doi.org/10.1111/j.1472-8206.2005.00316.x>.
32. Kapoor M, Martel-Pelletier J, Lajeunesse D, Pelletier JP, Fahmi H. Role of proinflammatory cytokines in the pathophysiology of osteoarthritis. *Nat Rev Rheumatol* 2011; 7:33-42; PMID:21119608; <http://dx.doi.org/10.1038/nrrheum.2010.196>.
33. Bertone AL, Palmer JL, Jones J. Synovial fluid cytokines and eicosanoids as markers of joint disease in horses. *Vet Surg* 2001; 30:528-38; PMID:11704948; <http://dx.doi.org/10.1053/jvet.2001.28430>.
34. Ritchlin C. Fibroblast biology. Effector signals released by the synovial fibroblast in arthritis. *Arthritis Res* 2000; 2:356-60; PMID:11094448; <http://dx.doi.org/10.1186/ar112>.
35. Attur M, Samuels J, Krasnokutsky S, Abramson SB. Targeting the synovial tissue for treating osteoarthritis (OA): where is the evidence? *Best Pract Res Clin Rheumatol* 2010; 24:71-9; PMID:20129201; <http://dx.doi.org/10.1016/j.berh.2009.08.011>.
36. Byron CR, Stewart MC, Stewart AA, Ponden HC. Effects of clinically relevant concentrations of glucosamine on equine chondrocytes and synoviocytes in vitro. *Am J Vet Res* 2008; 69:1129-34; PMID:18764682; <http://dx.doi.org/10.2460/ajvr.69.9.1129>.
37. May SA, Hooke RE, Lees P. Interleukin-1 stimulation of equine articular cells. *Res Vet Sci* 1992; 52:342-8; PMID:1620968; [http://dx.doi.org/10.1016/0034-5288\(92\)90035-Z](http://dx.doi.org/10.1016/0034-5288(92)90035-Z).
38. Hardy J, Bertone AL, Weisbrode SE, Muir WW, O'Dorisio TM, Masty J. Cell trafficking, mediator release, and articular metabolism in acute inflammation of innervated or denervated isolated equine joints. *Am J Vet Res* 1998; 59:88-100; PMID:9442251.
39. Pearson W, Orth MW, Lindinger MI. Evaluation of inflammatory responses induced via intra-articular injection of interleukin-1 in horses receiving a dietary nutraceutical and assessment of the clinical effects of long-term nutraceutical administration. *Am J Vet Res* 2009; 70:848-61; PMID:19566470; <http://dx.doi.org/10.2460/ajvr.70.7.848>.
40. Sabaratnam S, Coleman PJ, Mason RM, Levick JR. Interstitial matrix proteins determine hyaluronan reflection and fluid retention in rabbit joints: effect of protease. *J Physiol* 2007; 578:291-9; PMID:17008373; <http://dx.doi.org/10.1113/jphysiol.2006.119446>.
41. Zuin S, Pojana G, Marcomini A. Effect-Oriented Physicochemical Characterization of Nanomaterials. In: Monteiro-Riviere NA, Tran CL, eds. *Nanotoxicology: Characterization, Dosing and Health Effects*. New York: Informa Healthcare, 2007:19-57.
42. Stone V, Kinloch I. Nanoparticle Interactions with Biological Systems and Subsequent Activation of Intracellular Signaling Mechanisms. In: Monteiro-Riviere NA, Tran CL, eds. *Nanotoxicology: Characterization, Dosing and Health Effects*. New York: Informa Healthcare, 2007:351-68.
43. Brewer SH, Glomm WR, Johnson MC, Knag MK, Franzen S. Probing BSA binding to citrate-coated gold nanoparticles and surfaces. *Langmuir* 2005; 21:9303-7; PMID:16171365; <http://dx.doi.org/10.1021/la050588t>.
44. Mahl D, Greulich C, Meyer-Zaika W, Koller M, Epple M. Gold nanoparticles: dispersibility in biological media and cell-biological effect. *J Mater Chem* 2010; 20:6176-81; <http://dx.doi.org/10.1039/c0jm01071e>.
45. Kroll A, Pillukat MH, Hahn D, Schneckeburger J. Current in vitro methods in nanoparticle risk assessment: limitations and challenges. *Eur J Pharm Biopharm* 2009; 72:370-7; PMID:18775492; <http://dx.doi.org/10.1016/j.ejpb.2008.08.009>.
46. Monteiro-Riviere NA, Inman AO, Zhang LW. Limitations and relative utility of screening assays to assess engineered nanoparticle toxicity in a human cell line. *Toxicol Appl Pharmacol* 2009; 234:222-35; PMID:18983864; <http://dx.doi.org/10.1016/j.taap.2008.09.030>.
47. Kroll A, Pillukat MH, Hahn D, Schneckeburger J. Interference of engineered nanoparticles with in vitro toxicity assays. *Arch Toxicol* 2012; 86:1123-36; PMID:22407301; <http://dx.doi.org/10.1007/s00204-012-0837-z>.
48. Wang G, Zhang J, Dewilde AH, Pal AK, Bello D, Therrien JM, et al. Understanding and correcting for carbon nanotube interferences with a commercial LDH cytotoxicity assay. *Toxicology* 2012; 299:99-111; PMID:22634321; <http://dx.doi.org/10.1016/j.tox.2012.05.012>.
49. Wang Z, Zhao J, Li F, Gao D, Xing B. Adsorption and inhibition of acetylcholinesterase by different nanoparticles. *Chemosphere* 2009; 77:67-73; PMID:19540550; <http://dx.doi.org/10.1016/j.chemosphere.2009.05.015>.
50. Hyc A, Osiecka-Iwan A, Niderla-Bielinska J, Jankowska-Steifer E, Moskalewski S. Pro- and anti-inflammatory cytokines increase hyaluronan production by rat synovial membrane in vitro. *Int J Mol Med* 2009; 24:579-85; PMID:19724900.
51. Tammi RH, Passi AG, Rilla K, Karousou E, Vignetti D, Makkonen K, et al. Transcriptional and post-translational regulation of hyaluronan synthesis. *FEBS J* 2011; 278:1419-28; PMID:21362137; <http://dx.doi.org/10.1111/j.1742-4658.2011.08070.x>.
52. Sumbayev VV, Yasinska IM, Garcia CP, Gilliland D, Lall GS, Gibbs BF, et al. Gold nanoparticles down-regulate interleukin-1 $\beta$ -induced pro-inflammatory responses. *Small* 2013; 9:472-7; PMID:23112137; <http://dx.doi.org/10.1002/smll.201201528>.
53. Bhattacharya R, Mukherjee P, Xiong Z, Atala A, Soker S, Mukhopadhyay D. Gold nanoparticles inhibit VEGF165-induced proliferation of HUVEC cells. *Nano Lett* 2004; 4:2479-81; <http://dx.doi.org/10.1021/nl0483789>.
54. Ma JS, Kim WJ, Kim JJ, Kim TJ, Ye SK, Song MD, et al. Gold nanoparticles attenuate LPS-induced NO production through the inhibition of NF-kappaB and IFN-beta/STAT1 pathways in RAW264.7 cells. *Nitric Oxide* 2010; 23:214-9; PMID:20547236; <http://dx.doi.org/10.1016/j.niox.2010.06.005>.
55. Larsen A, Stoltenberg M, Danscher G. In vitro liberation of charged gold atoms: autoradiographic tracing of gold ions released by macrophages grown on metallic gold surfaces. *Histochem Cell Biol* 2007; 128:1-6; PMID:17549510; <http://dx.doi.org/10.1007/s00418-007-0295-5>.

56. Elder RC, Zhao Z, Zhang YF, Dorsey JG, Hess EV, Tepperman K. Dicyanogold (I) is a common human metabolite of different gold drugs. *J Rheumatol* 1993; 20:268-72; PMID:8474063.
57. Graham GG, Dale MM. The activation of gold complexes by cyanide produced by polymorphonuclear leukocytes--II. Evidence for the formation and biological activity of aurocyanide. *Biochem Pharmacol* 1990; 39:1697-702; PMID:2160818; [http://dx.doi.org/10.1016/0006-2952\(90\)90113-Y](http://dx.doi.org/10.1016/0006-2952(90)90113-Y).
58. Graham GG, Kettle AJ. The activation of gold complexes by cyanide produced by polymorphonuclear leukocytes. III. The formation of aurocyanide by myeloperoxidase. *Biochem Pharmacol* 1998; 56:307-12; PMID:9744567; [http://dx.doi.org/10.1016/S0006-2952\(98\)00031-8](http://dx.doi.org/10.1016/S0006-2952(98)00031-8).
59. Yanni G, Nabil M, Farahat MR, Poston RN, Panayi GS. Intramuscular gold decreases cytokine expression and macrophage numbers in the rheumatoid synovial membrane. *Ann Rheum Dis* 1994; 53:315-22; PMID:8017985; <http://dx.doi.org/10.1136/ard.53.5.315>.
60. Yang JP, Merin JP, Nakano T, Kato T, Kitade Y, Okamoto T. Inhibition of the DNA-binding activity of NF-kappa B by gold compounds in vitro. *FEBS Lett* 1995; 361:89-96; PMID:7890047; [http://dx.doi.org/10.1016/0014-5793\(95\)00157-5](http://dx.doi.org/10.1016/0014-5793(95)00157-5).
61. Yoshida S, Kato T, Sakurada S, Kurono C, Yang JP, Matsui N, et al. Inhibition of IL-6 and IL-8 induction from cultured rheumatoid synovial fibroblasts by treatment with aurothioglucose. *Int Immunol* 1999; 11:151-8; PMID:10069413; <http://dx.doi.org/10.1093/intimm/11.2.151>.
62. Nieminen R, Korhonen R, Moilanen T, Clark AR, Moilanen E. Aurothiomalate inhibits cyclooxygenase 2, matrix metalloproteinase 3, and interleukin-6 expression in chondrocytes by increasing MAPK phosphatase 1 expression and decreasing p38 phosphorylation: MAPK phosphatase 1 as a novel target for anti-rheumatic drugs. *Arthritis Rheum* 2010; 62:1650-9; PMID:20178133; <http://dx.doi.org/10.1002/art.27409>.
63. Tomlinson JE, Blikslager AT. Effects of cyclooxygenase inhibitors flunixin and deracoxib on permeability of ischaemic-injured equine jejunum. *Equine Vet J* 2005; 37:75-80; PMID:15651739; <http://dx.doi.org/10.2746/0425164054406865>.
64. Hill TL. A Canine Gastric Mucosa Injury Model. Raleigh, North Carolina: North Carolina State University, 2012.
65. Chang CC, Hsieh MS, Liao ST, Chen YH, Cheng CW, Huang PT, et al. Hyaluronan regulates PPAR $\gamma$  and inflammatory responses in IL-1 $\beta$ -stimulated human chondrosarcoma cells, a model for osteoarthritis. *Carbohydr Polym* 2012; 90:1168-75; PMID:22840054; <http://dx.doi.org/10.1016/j.carbpol.2012.06.071>.
66. Ross TN, Kisiday JD, Hess T, Mellwraith CW. Evaluation of the inflammatory response in experimentally induced synovitis in the horse: a comparison of recombinant equine interleukin 1 beta and lipopolysaccharide. *Osteoarthritis Cartilage* 2012; 20:1583-90; PMID:22917743; <http://dx.doi.org/10.1016/j.joca.2012.08.008>.
67. Sonavane G, Tomoda K, Makino K. Biodistribution of colloidal gold nanoparticles after intravenous administration: effect of particle size. *Colloids Surf B Biointerfaces* 2008; 66:274-80; PMID:18722754; <http://dx.doi.org/10.1016/j.colsurfb.2008.07.004>.
68. Sonavane G, Tomoda K, Sano A, Ohshima H, Terada H, Makino K. In vitro permeation of gold nanoparticles through rat skin and rat intestine: effect of particle size. *Colloids Surf B Biointerfaces* 2008; 65:1-10; PMID:18499408; <http://dx.doi.org/10.1016/j.colsurfb.2008.02.013>.
69. Khlebtsov N, Dykman L. Biodistribution and toxicity of engineered gold nanoparticles: a review of in vitro and in vivo studies. *Chem Soc Rev* 2011; 40:1647-71; PMID:21082078; <http://dx.doi.org/10.1039/c0cs00018c>.
70. Cho WS, Kim S, Han BS, Son WC, Jeong J. Comparison of gene expression profiles in mice liver following intravenous injection of 4 and 100 nm-sized PEG-coated gold nanoparticles. *Toxicol Lett* 2009; 191:96-102; PMID:19695318; <http://dx.doi.org/10.1016/j.toxlet.2009.08.010>.
71. Cho WS, Cho M, Jeong J, Choi M, Cho HY, Han BS, et al. Acute toxicity and pharmacokinetics of 13 nm-sized PEG-coated gold nanoparticles. *Toxicol Appl Pharmacol* 2009; 236:16-24; PMID:19162059; <http://dx.doi.org/10.1016/j.taap.2008.12.023>.
72. Hellstern D, Schulze K, Schöpf B, Petri-Fink A, Steitz B, Kamau S, et al. Systemic distribution and elimination of plain and with Cy3.5 functionalized poly(vinyl alcohol) coated superparamagnetic maghemite nanoparticles after intraarticular injection in sheep in vivo. *J Nanosci Nanotechnol* 2006; 6:3261-8; PMID:17048545; <http://dx.doi.org/10.1166/jnn.2006.482>.
73. Barber PA, Rushforth D, Agrawal S, Tuor UI. Infrared optical imaging of matrix metalloproteinases (MMPs) up regulation following ischemia reperfusion is ameliorated by hypothermia. *BMC Neurosci* 2012; 13:76; PMID:22742423; <http://dx.doi.org/10.1186/1471-2202-13-76>.
74. Dykstra MJ. *Manual of Applied Techniques for Biological Electron Microscopy*. New York, NY: Plenum Press, 1993.